



Hydrothermal synthesis of $\text{Ca}_3\text{Bi}_8\text{O}_{15}$ rods and their visible light photocatalytic properties

Wenjuan Li, Desheng Kong, Xiaoli Cui, Dandan Du, Tingjiang Yan, Jinmao You*

Shandong Province Key Laboratory of Life-Organic Analysis, Qufu Normal University, Qufu 273165, PR China

ARTICLE INFO

Article history:

Received 1 June 2013

Received in revised form 2 November 2013

Accepted 2 December 2013

Available online 8 December 2013

Keywords:

A. Inorganic compounds

B. Chemical synthesis

D. Catalytic properties

ABSTRACT

High efficient visible light $\text{Ca}_3\text{Bi}_8\text{O}_{15}$ photocatalysts were synthesized by a hydrothermal method. Characterized by X-ray diffractometer, transmission electron microscopy, and the UV–vis diffuse reflectance spectroscopy, the results showed that the novel $\text{Ca}_3\text{Bi}_8\text{O}_{15}$ rods can utilize the sunlight efficiently with the small band-gap. Using methyl orange (MO) as a model organic pollutant, the photocatalysts exhibited good photocatalytic activity, with the photodegradation conversion ratio of MO being up to 90% after 2 h of visible light ($420 \text{ nm} < \lambda < 800 \text{ nm}$) irradiation. Furthermore, they also showed good photocatalytic activities in the degradation of rhodamine B and p-chlorophenol. Through the investigation of the degraded mechanism, the main active species played important roles in the degradation process were holes, $\text{O}_2^{\cdot-}$ and $^{\cdot}\text{OH}$.

© 2013 Elsevier Ltd. All rights reserved.

1. Introduction

Photocatalytic oxidation technology using solar energy has been applied to a variety of problems of environmental interest in addition to water and air purification and considered as an ultimate approach to solve both energy and environmental problems [1]. The semiconductor TiO_2 has proven to be an excellent photocatalyst material in these fields [2–4]. However, it can only absorb a very small ultraviolet part (3–4%) of the solar light because of its wide band-gap (3.2 eV for anatase). So the extensive applications of titanium dioxide as an efficient photocatalyst are constrained. Many modification methods such as metal ion doping, composite semiconductors and metal layer modification have been used to extend the light absorption of the catalyst into the visible light region but have little effect [4–7]. Some traditional visible-light photocatalysts were either unstable upon illumination with light (e.g. CdS, CdSe) [8] or exhibited low activity (e.g. WO_3 , Fe_2O_3) [9]. How to efficiently exploit visible light active photocatalysts for degradation of environment pollutants with high quantum efficiency and high stability is the top goal at present even in future years.

Some Bi-base photocatalysts owning the small band gap have attracted much attention due to their strong absorption in the visible light region. They have been broadly applied in the photocatalytic water splitting into hydrogen and the degradation of organic pollutants [10–13]. Among them, the most widely

researching photocatalysts were BiVO_4 [11], Bi_2WO_6 [12], Bi_2MoO_6 [13], etc. However, the reports referred to $\text{Ca}_3\text{Bi}_8\text{O}_{15}$ photocatalysts were few in which they were synthesized by high-temperature solid-state method and their activities were lower [10,14]. Therefore, aimed at the development of the photocatalysts with high activity that are sensitive to visible light, we reported a new chemical approach to synthesize $\text{Ca}_3\text{Bi}_8\text{O}_{15}$ rods by a hydrothermal process using stable, inorganic salts CaSO_4 and Na_2BiO_3 as the reactants without any templates. And their photocatalytic activities in the degradation of organic pollutants such as methyl orange (MO), p-chlorophenol (4-CP) and rhodamine B (RhB) under visible light irradiation have been investigated in detail. The mechanism of the degradation processes was also explored.

2. Experimental

2.1. One step preparation of $\text{Ca}_3\text{Bi}_8\text{O}_{15}$ photocatalysts

First, an appropriate amount of analytical grade CaSO_4 (0.041 g) and $\text{NaBiO}_3 \cdot 2\text{H}_2\text{O}$ (0.474 g) according to a certain ratio were dissolved in deionized water (50 ml) to form a mixture solution. The pH value was adjusted by 2 M HNO_3 or NaOH . After stirring for 0.5 h, the solution was transferred to the Teflon liner with 100 ml capacity. The Teflon liner was then sealed in the stainless steel autoclave and maintained at a certain temperature for different hours. After the autoclave cooling naturally to ambient temperature, the resultant products were washed with water/ethanol for several times and then dried at 80°C for 12 h. All hydrothermal treatments were made in the absence of any dispersion or capping organic agent.

* Corresponding author. Tel.: +86 537 4458301; fax: +86 537 4458301.
E-mail address: jmyou6304@163.com (J. You).

2.2. Characterization of photocatalysts

Transmission electron microscopy (TEM) images were collected by using a JEOL JEM 2010F microscope working at 200 kV and equipped with an energy-dispersive X-ray analyzer (Phoenix). X-ray diffraction (XRD) patterns were recorded on a Bruker D8 Advance X-ray diffractometer with $\text{CuK}\alpha$ radiation. The UV-vis spectra of various liquid samples and diffuse reflectance spectra (DRS) were performed on Beijing Puxi TU1801 UV-vis spectrophotometer and Varian Cary 500 UV-vis spectrophotometer with an integrating sphere attachment ranging from 200 to 800 nm, respectively. X-ray photoelectron spectroscopy (XPS) analysis was conducted on an ESCALAB 250 photoelectron spectroscopy (Thermo Fisher Scientific Inc.) at 3.0×10^{-10} mbar with monochromatic $\text{AlK}\alpha$ Radiation ($E = 1486.2$ eV). The generation of hydroxyl radicals was investigated by the method of photoluminescence technique with terephthalic acid (PL-TA) [15]. The photoluminescence spectra were surveyed by Hitachi F4600 spectrometer. Photoelectrochemical measurements were performed in an H-type two-compartment, three-electrode cell, with a fine porous glass frit between the two compartments and with a 3.5-cm diameter quartz window for light illumination. The potential and current of the photoelectrode were controlled/recorded by an EG&G Princeton Applied Research Potentiostat/Galvanostat (PAR model 283) through PowerSuite software. The catalyst was deposited as a film form on a 1 cm \times 1 cm indium-tin-oxide conducting glass served as working electrode, the saturated calomel electrode (SCE) as the reference electrode, and Pt as the counter electrode. The electrolyte was 0.1 M Na_2SO_4 aqueous solution.

2.3. Tests of photocatalytic activity

The visible-light source was a 500 W halogen lamp (Philips Electronics) positioned beside a cylindrical reaction vessel with a plane side. Two cutoff filters (420 and 800 nm) were placed before the vessel to ensure that irradiation of the degradation system occurred only by visible-light wavelengths. The photo energy density was $230 \mu\text{W}/\text{cm}^2$. The overall system was cooled by wind and water to maintain the room temperature. A 0.04 g portion of catalysts was added to 80 ml MO (6.1×10^{-5} M), 4-CP (3×10^{-4} M) and RhB (3×10^{-4} M) solution in a 100 ml Pyrex glass vessel, respectively. Prior to irradiation, the suspensions were magnetically stirred in the dark for 1 h to ensure the equilibrium of

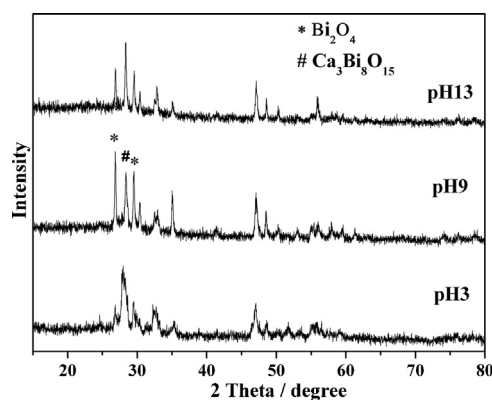


Fig. 1. XRD patterns of the samples prepared at different pH values.

the working solution. After irradiation, at given time intervals, 3 ml aliquots were sampled and centrifuged to remove the catalysts. The degraded solution was analyzed using a Beijing Puxi TU1801 UV-vis spectrophotometer and the maximum absorption peak was monitored. After degradation, the catalysts were centrifuged from the suspensions and dried for the following compared experiments.

3. Results and discussion

3.1. Physicochemical properties of $\text{Ca}_3\text{Bi}_8\text{O}_{15}$

Fig. 1 showed XRD patterns of the samples prepared at different pH values under the condition: $T = 120^\circ\text{C}$, $t = 24$ h. It indicated that as the pH = 3, the sample was $\text{Ca}_3\text{Bi}_8\text{O}_{15}$, in line with the standard spectra (JCPDS, card no. 48-0214). When the pH changed, Bi_2O_4 (JCPDS50-0864) appeared in the products. For example, when pH = 9 or 13, the as-prepared samples were the mixture of $\text{Ca}_3\text{Bi}_8\text{O}_{15}$ and Bi_2O_4 . Therefore, the appropriate synthesized pH value was 3.

Fig. 2(a) indicates that $\text{Ca}_3\text{Bi}_8\text{O}_{15}$ sample was composed of a large quantity of rods with diameter about 200 nm. The high-resolution TEM (HRTEM) in Fig. 2(b) shows the lattice fringes of $d = 0.31$ nm allowed for identification of the (0 0 3) planes for crystallographic spacing of $\text{Ca}_3\text{Bi}_8\text{O}_{15}$. The selected-area electron diffraction (SAED) pattern taken along a randomly selected single rod indicated that these rods were single crystalline.

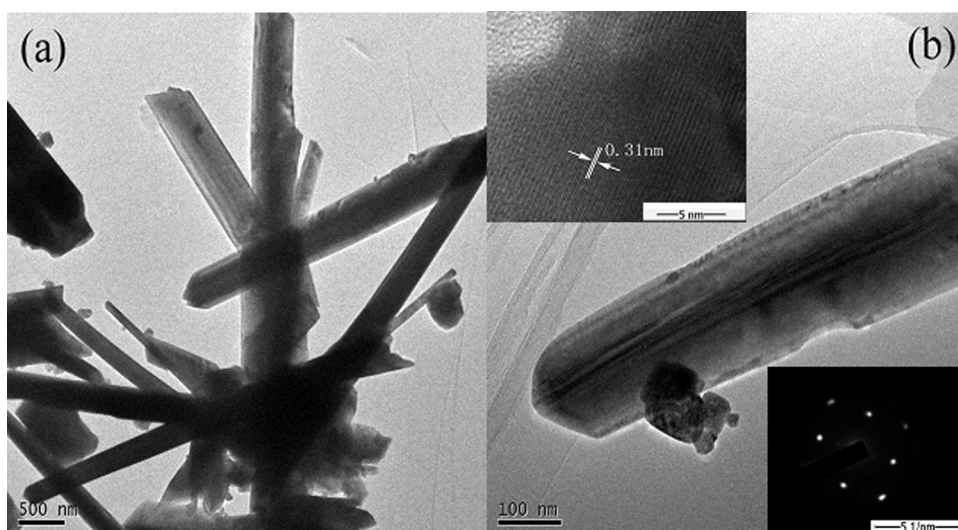


Fig. 2. (a) Low-magnification TEM, (b) high-magnification TEM, high-resolution TEM image and selected-area electron diffraction pattern of the $\text{Ca}_3\text{Bi}_8\text{O}_{15}$ rods.

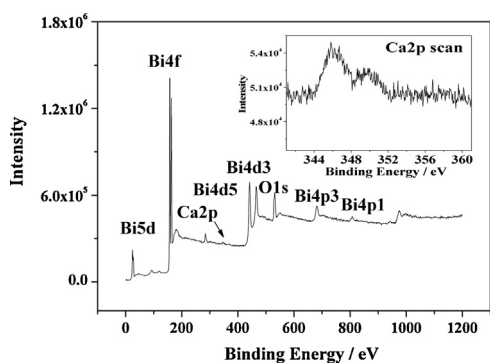


Fig. 3. XPS spectra of $\text{Ca}_3\text{Bi}_8\text{O}_{15}$.

From the detection of XPS (Fig. 3), the binding energies of 30, 159, 443, 465, 533, 680 and 810 eV were corresponding to Bi5d, Bi4f, Bi4d5, Bi4d3, O1s, Bi4p3 and Bi4p1, which were similar to those on $\beta\text{-Bi}_2\text{O}_3$. It indicated that the valence state of Bi was +3. The peak at 346 eV belonged to Ca2p. Thus, the as-prepared sample involved the elements of Ca, Bi, and O.

Fig. 4 shows the UV–vis DRS of $\text{Ca}_3\text{Bi}_8\text{O}_{15}$. From this figure, the as-prepared $\text{Ca}_3\text{Bi}_8\text{O}_{15}$ can absorb much visible light and the small band gap resulted in its absorption moving toward infrared region. It indicated that this sample could apply the sunlight efficiently which was favorable for the photocatalytic activity.

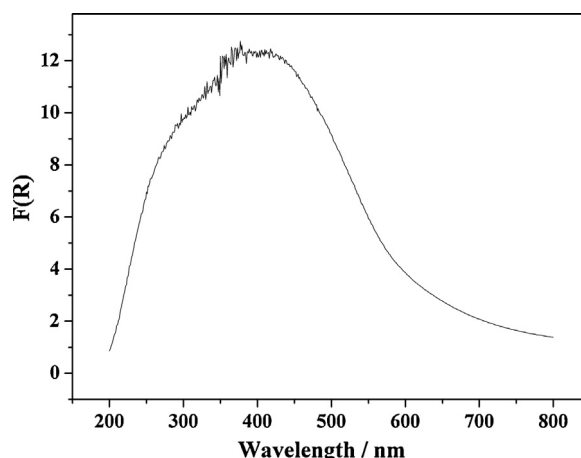


Fig. 4. UV–vis DRS of $\text{Ca}_3\text{Bi}_8\text{O}_{15}$.

3.2. Photocatalytic activity of $\text{Ca}_3\text{Bi}_8\text{O}_{15}$

The photocatalytic activity of $\text{Ca}_3\text{Bi}_8\text{O}_{15}$ under visible light irradiation was evaluated by the degradation of MO, RhB and 4-CP as the model. As shown in Fig. 5, after 120 min of irradiation under visible light ($420 \text{ nm} < \lambda < 800 \text{ nm}$), the photodegradation conversion ratio (PCR) of MO in the presence of $\text{Ca}_3\text{Bi}_8\text{O}_{15}$ sample was up to 90%. It was superior to that of $\text{TiO}_{2-x}\text{N}_x$ (prepared according to the Ref. [5]). Furthermore, it also showed good photocatalytic

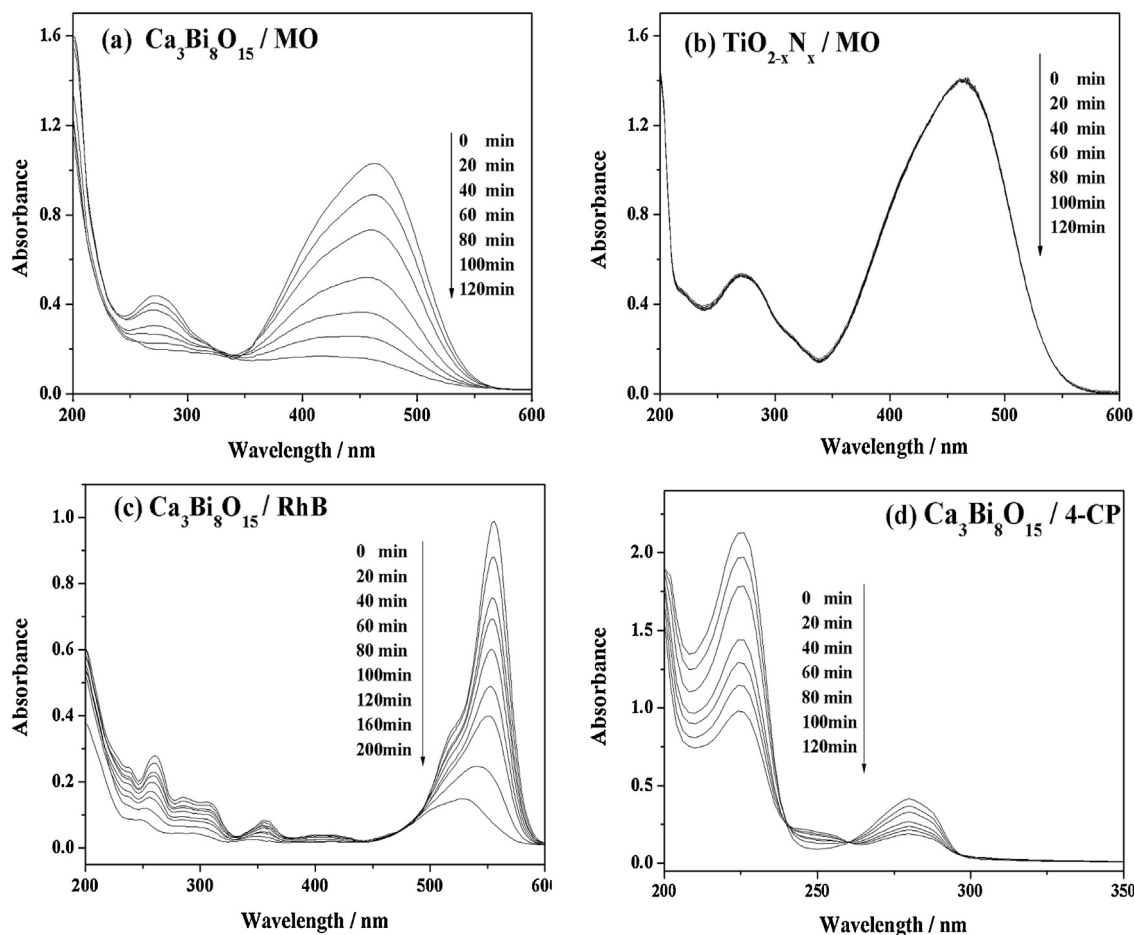


Fig. 5. Photocatalytic activity in the degradation of MO on (a) $\text{Ca}_3\text{Bi}_8\text{O}_{15}$ and (b) $\text{TiO}_{2-x}\text{N}_x$; Photocatalytic activity in the degradation of (c) RhB and (d) 4-CP on $\text{Ca}_3\text{Bi}_8\text{O}_{15}$ under exposure to visible light.

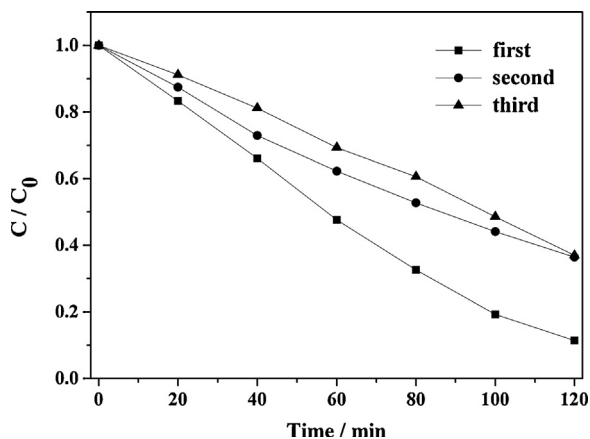


Fig. 6. The degradation rate of cycling runs for the photodegradation of MO in the presence of $\text{Ca}_3\text{Bi}_8\text{O}_{15}$ under visible light irradiation.

activity in the degradation of RhB and 4-CP. After 200 min of irradiation, the PCR of RhB achieved to 60%. As for 4-CP, the PCR was 55% after 120 min of irradiation. Therefore, the $\text{Ca}_3\text{Bi}_8\text{O}_{15}$ photocatalyst exhibited a good activity toward the organic pollutants under visible light irradiation.

We also tested the stability of $\text{Ca}_3\text{Bi}_8\text{O}_{15}$ sample through the detection of the degradation rate of cycling runs for the photodegradation of MO. In Fig. 6, although the conversion ratios of the second and third cycling runs for the photodegradation are decreased, the sample still remains a certain activity after the third

run. After 120 min of irradiation, the PCR of MO in the presence of $\text{Ca}_3\text{Bi}_8\text{O}_{15}$ was still up to 60%. Furthermore, the recycled sample after degradation of MO was also investigated and compared with the fresh one by XRD and XPS. Fig. 7a shows the XRD patterns of the samples before and after degradation. It indicated that the patterns had no obvious change. From the detection of XPS (Fig. 7b), the binding energies of the elements before and after degradation are nearly the same in the full survey spectra. It indicated that the $\text{Ca}_3\text{Bi}_8\text{O}_{15}$ sample possessed good chemical and mechanical stability.

3.3. Mechanism

The transfer of electrons in the photocatalytic process is very important, which would inhibit the recombination of electrons and holes and thus increase the activity. The separation of electrons and holes is always recognized to be the initial step in the photodegradation mechanism. Therefore, we first applied the electrochemical analysis to test the generation of photo-electrons. The photo-current line shown in Fig. 8 was tested in the 0.1 M Na_2SO_4 solution. At the appropriate electric potential with -0.1 V (chosen by the polarization curve, from Fig. 8b), the current generated and then reduced with the light on or off at a certain intervals. This result showed the generation of electrons in the photocatalytic process.

When the electrons were generated, separated with holes, they would transfer to the surface of the photocatalysts to engage in the oxidation–reduction reaction. In this process, some other active species with high activities generated and would also participate in

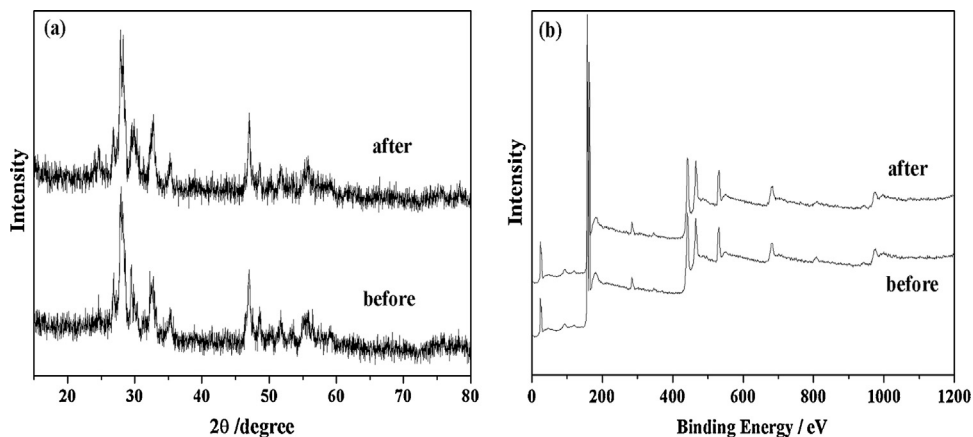


Fig. 7. The comparison of XRD and XPS of $\text{Ca}_3\text{Bi}_8\text{O}_{15}$ before and after degradation.

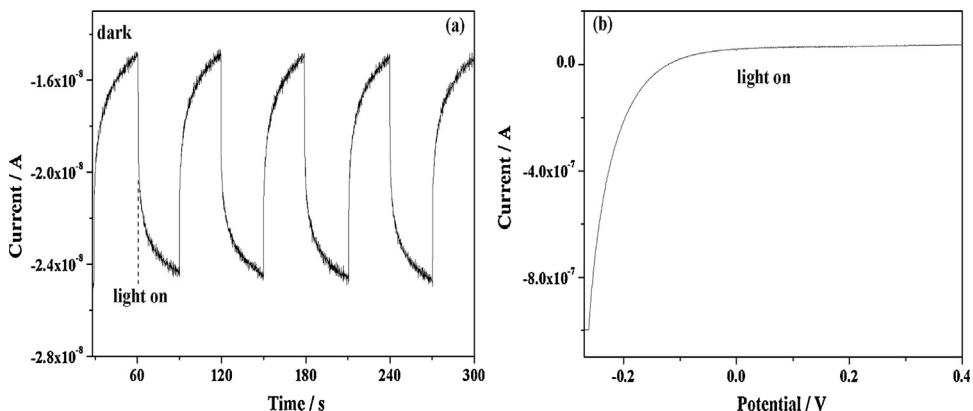


Fig. 8. (a) Photo-current line and (b) polarization curve of $\text{Ca}_3\text{Bi}_8\text{O}_{15}$ under visible light irradiation.

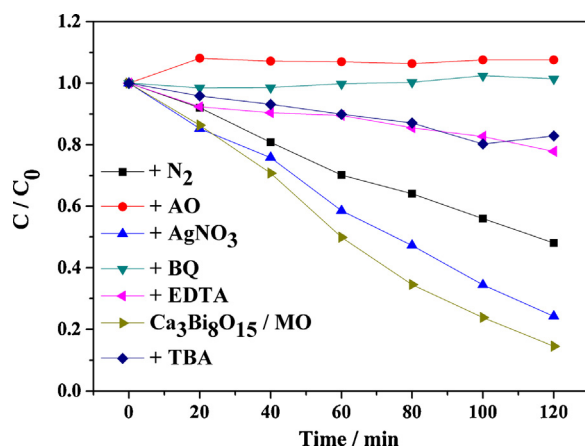


Fig. 9. The effect of different types of active species scavengers on the degradation of MO over $\text{Ca}_3\text{Bi}_8\text{O}_{15}$.

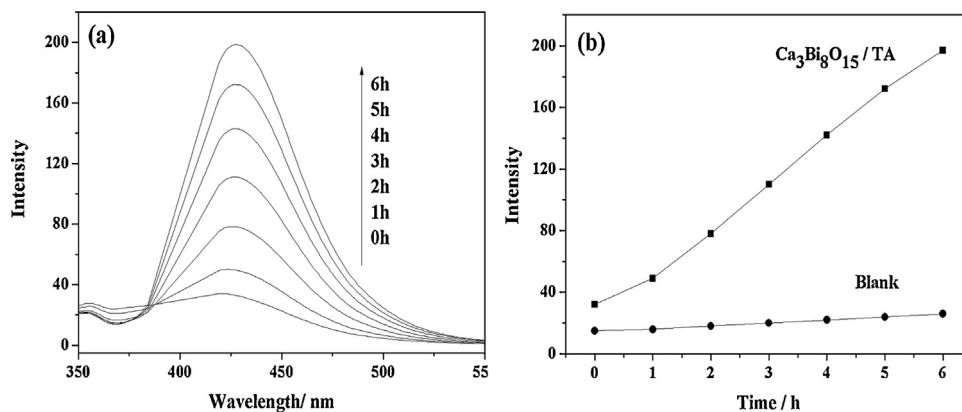


Fig. 10. (a) OH-trapping PL spectra of suspensions containing $\text{Ca}_3\text{Bi}_8\text{O}_{15}$ and TA, (b) changes of fluorescence intensity of the peak at $\lambda = 426 \text{ nm}$ with irradiation time.

the reaction. Therefore, the factors affecting the photocatalytic activity are related not only to the structure of materials, but also to the active species in the photodegradation process. We investigated the effect of the active species by adding some different types of scavengers in the degradation process of MO on $\text{Ca}_3\text{Bi}_8\text{O}_{15}$. The results were shown in Fig. 9. Ammonium oxalate (AO) and ethylene diamine tetraacetic acid (EDTA) are holes scavengers; benzoquinone (BQ) is $\text{O}_2^{\cdot-}$ scavenger; *tert*-butyl alcohol (TBA) is $\cdot\text{OH}$ scavenger. Compared with the activity in the absence of these scavengers, the effect of their adding was obvious. When N_2 was bubbled in the degradation system, the photocatalytic activity reduced which testified the effect of $\text{O}_2^{\cdot-}$. The addition of AgNO_3 , electron scavengers, had a little effect on the process and it showed the effect of electron was relatively small. In a word, the main active species played in the degradation process was holes, $\text{O}_2^{\cdot-}$ and $\cdot\text{OH}$, and then the electrons.

To further investigate the generation of $\cdot\text{OH}$, PL-TA technique was used in the detection. Fig. 10 shows the fluorescence spectra of suspensions containing $\text{Ca}_3\text{Bi}_8\text{O}_{15}$ and TA under visible light irradiation. It can be seen that the fluorescence intensity increased steadily with the irradiation time. Therefore, $\cdot\text{OH}$ radicals were indeed generated on $\text{Ca}_3\text{Bi}_8\text{O}_{15}$. Because of the generation of $\cdot\text{OH}$ radicals, the $\text{Ca}_3\text{Bi}_8\text{O}_{15}$ would possess the general applicability to degrade organic compounds other than dyes, such as 4-CP.

4. Conclusions

$\text{Ca}_3\text{Bi}_8\text{O}_{15}$ rods were prepared by a hydrothermal method without any templates, with the appropriate conditions: $T = 120 \text{ }^\circ\text{C}$, $t = 24 \text{ h}$, $\text{pH} = 3$. The photocatalysts can be applied in the degradation of MO, RhB and 4-CP. They showed high efficient

activities under visible light irradiation and obtained good stability. Through the exploration of the mechanism, it indicated that the main active species played in the degradation process were holes, $\text{O}_2^{\cdot-}$ and $\cdot\text{OH}$, and then the electrons. The further research about its mechanism should be proceeded.

Acknowledgments

This work is financially supported by the National Natural Science Foundation of China (21303094, 21275089 and 21103193), Natural Foundation of Shandong Province (ZR2010EM026), and Scientific Research Foundation of Qufu Normal University (XJ201213).

References

- [1] M.R. Hoffmann, S.T. Martin, W.Y. Choi, D.W. Bahnemann, *Chem. Rev.* 95 (1995) 69–96.
- [2] M.A. Fox, M.T. Dulay, *Chem. Rev.* 93 (1993) 341–357.
- [3] D.F. Ollis, E. Pelizzetti, N. Serpone, *Environ. Sci. Technol.* 25 (1991) 1522–1529.
- [4] J. Fan, J.T. Yates Jr., *J. Am. Chem. Soc.* 118 (1996) 4686–4692.
- [5] R. Asahi, T. Morikawa, T. Ohwaki, K. Aoki, Y. Taga, *Science* 293 (2001) 269–271.
- [6] S.U.M. Khan, M. Al-Shahry, W.B. Ingler Jr., *Science* 297 (2002) 2243–2245.
- [7] W. Zhao, W.H. Ma, C.C. Chen, J.C. Zhao, *J. Am. Chem. Soc.* 126 (2004) 4782–4783.
- [8] G.C. De, A.M. Roy, S.S. Bhattacharya, *Int. J. Hydrogen Energy* 20 (1995) 127–131.
- [9] D.W. Hwang, J. Kim, T.J. Park, J.S. Lee, *Catal. Lett.* 80 (2002) 53–57.
- [10] J. Tang, J. Ye, *Chem. Phys. Lett.* 410 (2005) 104–107.
- [11] L. Ge, X. Zhang, *J. Inorg. Mater.* 24 (2009) 453–456.
- [12] C. Zhang, Y.F. Zhu, *Chem. Mater.* 17 (2005) 3537–3545.
- [13] L. Zhang, T. Xu, X. Zhao, Y. Zhu, *Appl. Catal. B* 98 (2010) 138–146.
- [14] J.W. Xie, G.K. Zhang, Preparation of $\text{Ca}_8\text{Bi}_6\text{O}_{15}$ and Its Photocatalytic Properties, A Dissertation Submitted to Wuhan University of Technology for Master Degree, 2007.
- [15] J.T. Mason, P.J. Lorimer, M.D. Bates, Y. Zhao, *Ultrason. Sonochem.* 1 (1994) S91–S95.